Modification of Voltage-Dependent Gating of Potassium Channels by Free Form of Tryptophan Side Chain

Vladimir Avdonin and Toshinori Hoshi
Department of Physiology and Biophysics, The University of Iowa, Iowa City, Iowa 52242 USA

ABSTRACT Indole constitutes a major component of the side chain of the amino acid tryptophan. Application of indole slows activation of voltage-dependent potassium channels and reduces steady-state conductance in a voltage- and concentration-dependent manner. The steep concentration dependence indicates that multiple indole molecules may interact with the channel. Indole does not noticeably change the unitary conductance or the mean open duration, however, it accelerates off-gating currents without altering on-gating currents. These properties of the modification of channel gating induced by indole are consistent with a model in which indole binds independently to every subunit of the channel complex to prevent the final concerted transition to the open state. We suggest that exogenously applied indole and side-chains of the tryptophan residues of the channel protein involved in activation may compete for the same effector position and that indole might be useful as a probe to study functional roles of tryptophan residues.

INTRODUCTION

Tryptophan residues are highly conserved at several positions in different families of potassium channels and they may play important roles in the channel function. The crystal structure of the KcsA potassium channel shows that the stable conformation of the selectivity filter in the open state is maintained by a "massive sheet of aromatic amino acids, twelve in total, that are positioned like a cuff around the selectivity filter" (Doyle et al., 1998). This structure comprises a significant part of the framework constraining the selectivity filter in the optimal geometry to accommodate K^+ ions. Of the aromatic amino acid residues comprising this critical cuff-like structure, eight are tryptophan. The tryptophan residue at position 68 in the KcsA channel interacts directly with the tyrosine residue in the GYG K^+ channel pore signature sequence by forming a hydrogen bond (Doyle et al., 1998). Furthermore, given the bulkiness of these aromatic side chains, steric interactions are also important to stabilize the structure of the selectivity filter.

In addition to the role in ion conduction, the tryptophan residues around the selectivity filter segment may also contribute to activation- and inactivation-gating of K^+ channels. Several studies suggest that opening of the K^+ channel pore is associated with a major conformational rearrangement of the intracellular part of the channel (Holmgren et al., 1997; Liu et al., 1997; Yellen, 1998), which might involve the repositioning of tryptophan side chains. A site-directed spin labeling and electron paramagnetic resonance (EPR) spectroscopy study of gating of the KcsA channel indicates that the transition from the closed to the open state involves tilting and translation of the helixes forming the channel pore (Perozo et al., 1999). Although no obvious rearrangement is detected at the external side of the selectivity filter, the conformation of the lower part of the selectivity filter probably changes during gating (Perozo et al., 1999). This rearrangement might involve changes in steric contacts of tryptophan residues near the selectivity filter. Specifically, threonine at position 72 changes its steric contact during pH-dependent gating, and the side chain of this threonine residue projects toward tryptophan at position 68, sterically interacting with its side chain when the channel is open.

Mutation of the highly conserved tryptophan at position 434 in the pore segment of the ShB potassium channel to phenylalanine (W434F) renders the channel non-conducting while apparently preserving its ability to undergo voltage-dependent activation as revealed by gating current measurements (Perozo et al., 1993). Subsequent studies suggest that the W434F mutant channel may preferentially reside in a state characterized by altered ion selectivity and gating properties (Starkus et al., 1997) that closely resembles the C-type inactivated state of the wild type channel (Yang et al., 1997). Position 449 in the external mouth of the pore of the ShB channel is a major determinant in the rate of C-type inactivation (Lopez-Barneo et al., 1993). Homology modeling of the Shaker pore structure based on the KcsA structure (Guex and Peitsch, 1997) indicates that the side chain of the threonine residue at this position projects toward tryptophan at position 434, possibly interacting with its side chain.

The chemical and physical properties of the amino acid tryptophan are largely determined by the presence of the double-ring aromatic structure, called indole, in its side chain (Creighton, 1983) (Fig. 1 *A*). The indole structure is present in a variety of naturally occurring compounds such as serotonin (neurotransmitter), hypaphorine (convulsive poison), psilocin (hallucinogen), and heteroauxin (plant growth factor) (Windholz, 1976). Indolealkylamines are indole-based compounds known for their hallucinogenic

Received for publication 2 October 2000 and in final form 6 April 2001.
Address reprint requests to Toshinori Hoshi, Ph.D., Department of Physiology and Biophysics, Bowen 5660, The University of Iowa, Iowa City, IA 52242. Tel.: 319-335-7845; Fax: 319-353-5541; E-mail: hoshi@physiology.uiowa.edu.

0006-3495/01/07/97/10 $2.00

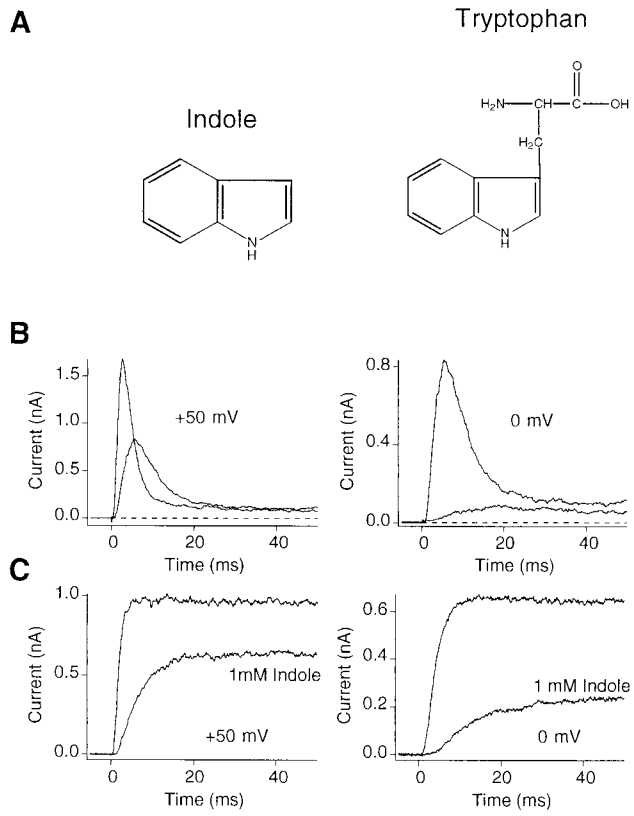

FIGURE 1 (*A*) Chemical structures of indole and tryptophan. (*B* and *C*) Representative recordings showing the effects of indole on Shaker potassium channels. The currents were recorded from inside-out patches. One mM indole was added to the bath solution. *Left panels* show currents recorded in response to depolarization to + 50 mV and *right panels* show the currents recorded at 0 mV. (*B*) ShB channel currents with fast N-type inactivation. (*C*) ShBΔ 6–46:T449V currents.

properties (Glennon and Rosecrans, 1982). In free form, indole is soluble in water in concentrations up to several mM. The mutagenesis and structural studies mentioned earlier led us to hypothesize that exogenously-applied indole and tryptophan side chains may compete for the same effector pocket within the channel protein, and alter those gating transitions mediated by repositioning of the tryptophan side chain. To test this hypothesis, we examined the effects of indole on Shaker potassium channels expressed in *Xenopus* oocytes.

MATERIALS AND METHODS

Channel expression

ShB, ShBΔ 6–46:T449V, and Kir2.1 channels were expressed in *Xenopus* oocytes by RNA injection as previously described (Hoshi et al., 1990; Kubo et al., 1993). The RNAs were transcribed using T7 RNA polymerase (Ambion, Austin, TX) and injected into the oocytes (45 nl/cell). Recordings were typically made 1 to 14 days after injection.

Electrophysiological recording

The macroscopic and single-channel recordings were performed as described (Hamill et al., 1981; Methfessel et al., 1986). The macroscopic patch currents were low-pass filtered at 2 kHz and digitized at 10 kHz using an ITC16 computer interface (Instrutech, Port Washington, NY). The data were collected and analyzed using Patch Machine (http://www.hoshi.org) and Igor Pro (Wavemetrics, Lake Oswego, OR) running on Apple Macintosh computers. Linear capacitative and leak currents have been subtracted from the macroscopic Shaker currents presented using the standard *P/6* protocol. Leak subtraction for gating currents was performed using a modified *P/n* protocol as implemented in Patch Machine (Fig. 6, legend). The single-channel and gating currents were filtered at 5 kHz and digitized at 25 kHz. When appropriate, the data values are presented as mean ± standard deviation. The error bars are not shown when smaller than the symbol size. All experiments were performed at room temperature (20–24°C).

Currents through Kir2.1 (IRK1) channels were recorded using the two-electrode voltage clamp (TEV) method with a Warner OC-725B amplifier (Warner, Hamden, CT). The electrodes filled with 3 M KCl had a typical initial resistance of <0.4 MΩ. The vitelline membrane of the oocyte was left intact. No leak subtraction was made for the Kir2.1 results.

The hidden Markov model (Chung and Gage, 1998) was used to idealize the single channel records. ShBΔ 6–46:T449V channels sometimes open to states with current amplitudes smaller than the full open channel current. These partial openings were accounted for by introducing a half amplitude sub-state into the hidden Markov model during the idealization process. Although there are likely to be multiple partial open states with different amplitudes (Zheng and Sigworth, 1998), this approach was adopted to distinguish the conducting states of the channel from the non-conducting states. Transitions between partially open states were ignored in the analysis, and all conducting single-channel events are considered to arise from one fully open state.

Solutions

The intracellular solution typically contained 140 mM KCl, 2 mM $MgCl_2$, 11 mM EGTA, 10 mM HEPES (pH 7.2) *N*-methyl glucamine (NMG). The standard extracellular solution contained 140 mM NaCl, 2 mM $MgCl_2$, 2 mM KCl, 10 mM HEPES (pH 7.2) NMG. For the gating current experiments, the extracellular solution contained 140 mM NMG, 2 mM $MgCl_2$, 10 mM HEPES (pH 7.2; HCl); and the intracellular solution contained 140 mM NMG, 2 mM $MgCl_2$, 10 mM HEPES, 11 mM EGTA (pH 7.2; HCl). Bath solution for recording of Kir2.1 inward-rectifier channel currents contained 140 mM KCl, 2 mM $MgCl_2$, 10 mM HEPES, pH 7.2 (NMG).

RESULTS

Indole suppresses ionic currents through Shaker K^+ channels.

The ionic currents through wild type ShB channels with intact N-type inactivation were reduced by application of 1 mM indole to the cytoplasmic side as shown in Fig. 1 *B*. At both 0 and 50 mV, indole noticeably decreased the peak current amplitudes. At 0 mV, the current was suppressed by $>85\%$, whereas at +50 mV, the peak current was reduced by ~50%, indicating that the inhibitory effect of indole may be voltage-dependent. To better study the mechanism of the indole action, we used the ShBΔ 6- 46:T449V channel. In this channel, a large deletion in the amino terminus (Δ

6–46) disrupts N-type inactivation (Hoshi et al., 1990) and the T449V mutation in the pore segment drastically slows C-type inactivation when expressed in *Xenopus* oocytes (Lopez-Barneo et al., 1993). Representative ShBΔ 6–46:T449V macroscopic currents recorded at 0 and 50 mV in the presence of indole are shown in Fig. 1 *C*. In comparison with the results obtained using wild type ShB channels with fast N-type inactivation, the relative reduction in the peak current amplitude caused by indole was noticeably smaller. At 50 and 0 mV, indole typically reduced the peak currents to ~60 and 30% of the control levels, respectively. The results using ShBΔ 6–46:T449V channels without fast inactivation revealed that indole not only decreased the peak current amplitude but also markedly slowed the activation time course. This phenomenon was further investigated as presented below. The onset of the effect of indole to alter the Shaker channel currents was rapid and the inhibitory effect was completely reversible by washing.

Indole effect has steep concentration dependence

Fig. 2 *A* shows ionic currents through ShBΔ 6–46:T449V channels recorded in the inside-out configuration in the presence of different concentrations of indole on the cytoplasmic side of the membrane. At 50 mV, indole (1 mM) reduced the current only to about 50%, whereas at 4 mM, the concentration only 4 times higher, the current was completely suppressed. The concentration dependence of the steady state block at 50 mV and 0 mV is shown in Fig. 2 *B*. Indole produced similar effects when applied from either side of the membrane but external application was somewhat more effective (Fig. 2 *B*).

The observation that indole is effective when applied from either side of the membrane is consistent with the possibility that the channel has one effector site, but indole could reach the site by traversing the membrane, making both internal and external applications effective. To test this idea, we applied 4 mM indole to the bath solution while recording the channel currents in the cell-attached configuration. Some dihydropyridine Ca^{2+} channel modulators, such as nifedipine, are known to be effective when applied in this manner because of their ability to cross the membrane and reach the channel proteins (Hess et al., 1984; Pang and Sperelakis, 1983). However, indole applied to the bath solution in the cell-attached configuration did not markedly alter the channel activity (data not shown). This result is consistent with the idea that indole does not cross the membrane appreciably to alter the channel currents and that the effector site(s) of the channel for the indole action may be readily accessible from either side of the membrane. This result, however, does not exclude the possibility that indole diffuses into the oocyte cytoplasm away from the channels.

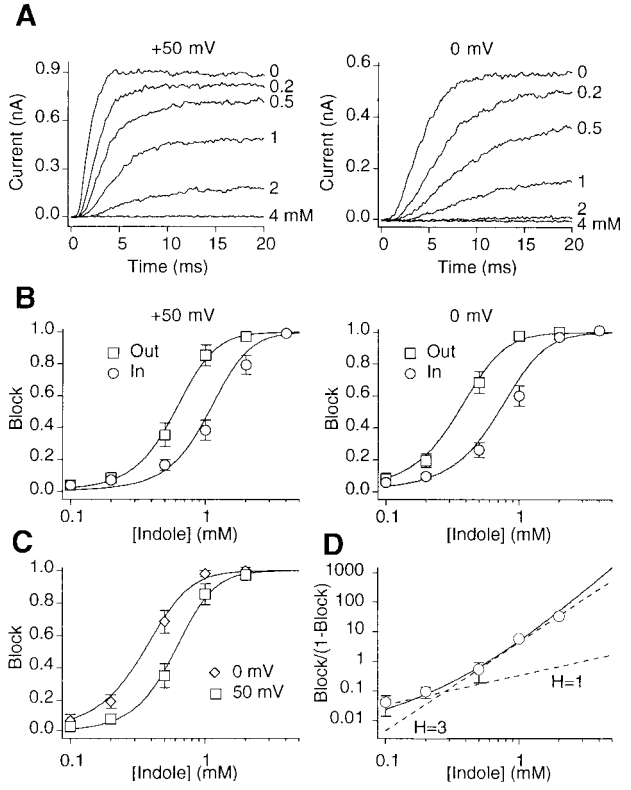

FIGURE 2 Concentration dependence of the indole effect. (*A*) A family of macroscopic ionic currents recorded with different concentrations of indole. The currents shown were recorded from an inside-out patch at 50 mV (*left*) and 0 mV (*right*). The indole concentrations in mM are shown next to the corresponding traces. (*B*) Steady-state block values measured at different concentrations of indole. The values were computed as ratio of current amplitudes reduction in the presence of indole to the respective current amplitudes in the control condition. The data were measured at +50 mV (*left*) and 0 mV (*right*). Each plot shows data for application of indole to cytoplasmic side of the membrane (inside-out patches, *circles*) and extracellular side (outside-out patches, *squares*). Data from five inside-out and six outside-out experiments were compiled. Smooth curves are best fits of the data using a model with four independent sequential binding steps described in Discussion. The dissociation constants for binding of a single indole molecule, determined by fitting experimental data with the model predictions, were 0.46 ± 0.03 mM (+50 mV) and 0.51 ± 0.03 mM (0 mV) for application of indole at the intracellular side, and 0.26 ± 0.02 mM at both +50 mV and 0 mV for indole applied at the extracellular side of the membrane. (*C*) Effect of voltage on concentration dependence of the steady state indole block. Data for extracellular application of indole at depolarization to 0 mV and 50 mV are shown. The data and smooth curves are the same as in *B*. (*D*) Steady state block values measured at +50 mV in outside-out configuration are plotted in Hill's coordinates. Data values and smooth curve are the same as shown in *B*. *Straight dotted lines* are predictions of a simple block model with a first (H = 1) and third (H = 3) molecular order.

The blocking effect of indole diminished with greater depolarization (Fig. 1, *B* and *C*). The concentration dependence of indole block at 0 mV and 50 mV is compared in Fig. 2 *C*. Greater depolarization caused the concentration dependence curve to shift to higher concentrations.

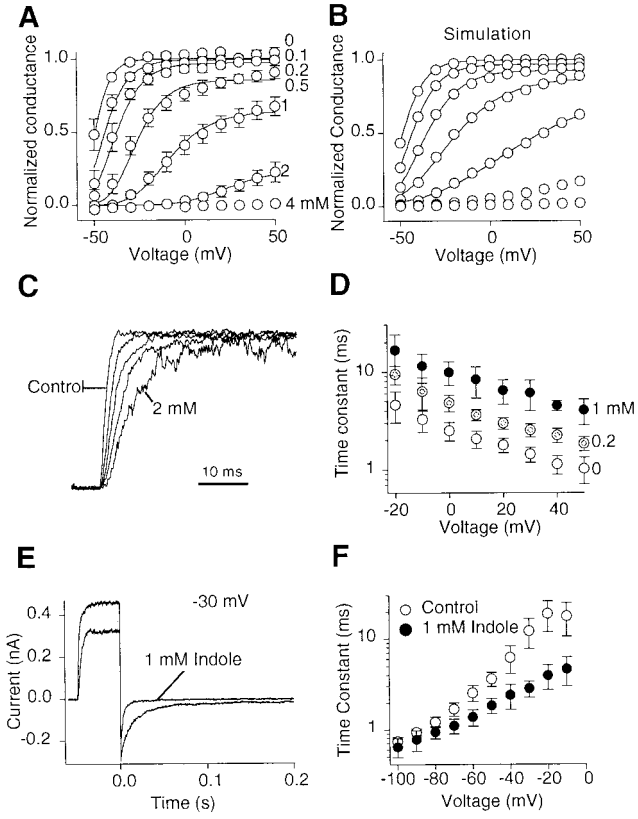

FIGURE 3 Indole effects on activation and deactivation of ShBΔ 6–46:T449V channel. (*A*) Voltage dependence of normalized steady-state conductance of ShBΔ 6–46:T449V in the presence of different concentrations of indole. Macroscopic chord conductance values are normalized to those in the control conditions. Recordings were made using the inside-out patch configuration with indole applied to the cytoplasmic side of the membrane. The indole concentrations in mM are shown next to the corresponding curves. Data points were averaged from five independent experiments. The smooth curves show the best fit of data with fourth power of a Boltzmann distribution. The parameters of fits are: control $V_h = -58 \pm 3$ mV, $z = 4.7 \pm 0.8$e; 0.1 mM $V_h = -57 \pm 3$ mV, $z = 3.2 \pm 0.5$e; 0.2 mM $V_h = -53 \pm 2$ mV, $z = 2.8 \pm 0.3$e; 0.5 mM $V_h = -43 \pm 2$ mV, $z = 2.5 \pm 0.3$e; 1 mM $V_h = -32 \pm 2$, $z = 1.8 \pm 0.3$e; 2 mM $V_h = -4 \pm 6$ mV, $z = 1.4 \pm 0.7$e. (*B*) Voltage dependence of normalized steady state conductance for simulated data. Current traces were numerically simulated using the model of indole effect described in discussion section. The graph was built following the same procedure as for *A*. The parameters of the Boltzmann fits are: control $V_h = -61$ mV, $z = 3.3$e; 0.1 mM $V_h = -58$ mV, $z = 2.7$e; 0.2 mM $V_h = -56$ mV, $z = 2.2$e; 0.5 mM $V_h = -53$ mV, $z = 1.4$e; 1 mM $V_h = -41$ mV, $z = 0.7$e. (*C*) Scaled representative sweeps showing the activation time course of ShBΔ 6–46:T449V in the presence of different concentrations of indole. Traces were recorded from the same inside-out patch and scaled to the steady state currents. Indole was applied to the cytoplasmic side of the membrane at the following concentrations (mM): 0, 0.2, 0.5, 1, and 2. Increasing indole concentrations progressively slowed activation, so that the intermediate traces from left to right correspond to the intermediate concentrations in the increasing order. The data traces were recorded at +50 mV depolarization. (*D*) Voltage dependence of the time constant of macroscopic current activation with different concentrations of indole. The time constant values were estimated by fitting the activation time course with an exponential after the current reached the half maximum amplitude. (*E*) Representative tail currents recorded from inside-out patch with external sodium replaced by potassium. Tail currents were recorded at −30 mV after 50 ms depolarization to +50 mM. The control trace is compared with the trace recorded in the presence of 1 mM indole on the cytoplasmic side of the membrane. (*F*) Voltage dependence of deactivation time course. Time constants of exponential fit of the tail currents in the control and in the presence of 1 mM indole on the cytoplasmic side. Tail currents were recorded at the voltages indicated after 50 ms depolarization to +50 mV ($n = 5$).

The steepness of the concentration dependence of indole block is greater than expected from those models that assume that the block is induced by binding of a single indole molecule. This property of the steady state block is more apparent when the concentration dependence is shown using Hill's coordinates, as in Fig. 2 *D*. The straight dashed lines on this plot show predictions of the first and third order reactions. The first order reaction has a significantly lower slope than that inferred from the experimental data. The line for the third order reaction better describes the experimental data at higher concentrations. The solid curve on this plot and smooth curves in Fig. 2, *B* and *C* show predictions of the model with independent bindings of four molecules of indole as described in the Discussion. The dissociation constant values for binding of a single indole molecule, determined by fitting the experimental data with this model, were 0.46 ± 0.03 mM (+50 mV) and 0.51 ± 0.03 mM (0 mV) for the intracellular indole application and 0.26 ± 0.02 mM at both +50 mV and 0 mV for indole applied to the extracellular side. Note that our model of the indole action does not postulate any intrinsic voltage dependence of the indole binding and the apparent voltage dependence is derived from the channel gating (see Discussion).

Indole decreases steady-state conductance in a voltage-dependent manner

As noted above, the blocking effect of indole decreases with membrane depolarization (Fig. 1, *B* and *C*). Fig. 3 *A* shows the voltage dependence of the normalized steady-state conductance of ShBΔ 6–46:T449V channels in the presence of different concentrations of indole on the cytoplasmic side. The macroscopic conductance was estimated from exponential fits to the tail currents at −60 mV following pulses to the voltages indicated on the abscissa long enough for the currents to reach steady-state. Indole decreased the voltage dependence of the macroscopic conductance such that changes in the overall conductance occurred over a much wider range of voltages. With high concentrations of indole (1, 2, and 4 mM), the voltage dependence became so shallow that the apparent maximal conductance in the measured voltage range was much lower than that in the control condition. The smooth lines in Fig. 3 *A* show best fits of the data with the 4th power of a Boltzmann distribution, which can be interpreted to mean that four identical and independent subunits may be involved in the channel activation process (Zagotta et al., 1994). The apparent gating charge

movement for each subunit derived from these fits decreased with increasing concentrations of indole, from 4.7 ± 0.5e ($n = 5$) in the control condition to 1.8 ± 0.3e ($n = 5$) with 1 mM indole. The half-activation voltage for each subunit also was affected, shifting from −58 ± 3 mV ($n = 5$) in the control condition to −32 ± 2 mV ($n = 5$) in the presence of 1 mM indole.

Indole slows activation time course

Scaled macroscopic currents recorded in the presence of different concentrations of indole at 50 mV are compared in Fig. 3 *C*. The results clearly show that indole slows the overall activation time course in a concentration-dependent manner. The voltage dependence of slowing of the activation time course by indole is illustrated in Fig. 3 *D*, where the time constants of activation at different voltages are shown. The late phase of the activation time course was fitted with a single exponential starting at the time when the current reached its half-maximal value (Schoppa and Sigworth, 1998a; Zagotta et al., 1994). Comparison of the voltage dependence of the overall macroscopic conductance (Fig. 3 *A*) and the activation time constant (Fig. 3 *D*) demonstrates that indole slows the activation time course even at those positive voltages where the macroscopic conductance in the control condition is saturated. Considering that the forward (opening) transitions dominate at the voltages where the macroscopic conductance is near saturation, the results suggest that indole interferes with the opening transitions.

Indole also accelerates deactivation time course

Indole markedly accelerated the deactivation time course of the ShBΔ 6–46:T449V channel. Representative tail currents recorded at −30 mV before and after indole application to the cytoplasmic side (1 mM) are shown in Fig. 3 *E*. The external solution contained high K^+ to better resolve the fast tail currents. The tail current time course was approximated by a single exponential and the time constant values estimated are shown as a function of voltage in Fig. 3 *F*. Acceleration of the tail current time course was most readily observed at depolarized voltages but the effect became progressively smaller with greater hyperpolarization.

Effects of indole on single-channel parameters

Representative single-channel openings recorded at 40 mV and 0 mV in the control condition and in the presence of indole (1 mM) on the cytoplasmic side are shown in Fig. 4 *A*. Indole application did not change the reversal potential but slightly decreased the single channel conductance as revealed by the openings elicited in response to voltage ramps (data not shown). The traces clearly show that the

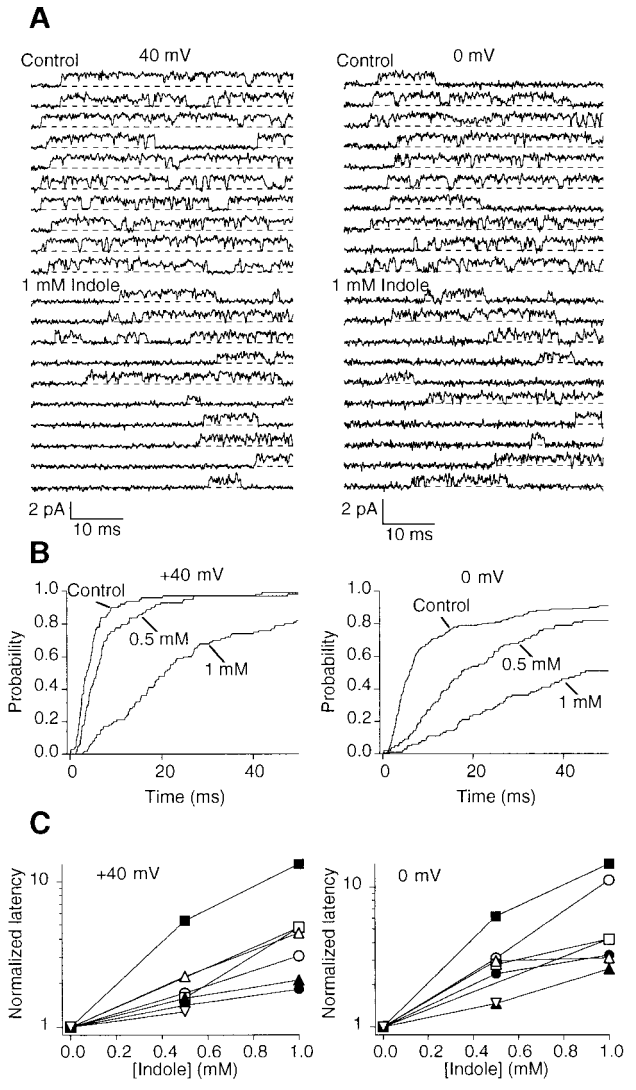

FIGURE 4 Indole effect on the first latency distribution of a single ShBΔ 6–46:T449V channel. (*A*) Representative openings of a ShBΔ 6–46:T449V recorded from an inside-out patch in the control and in the presence of 1 mM indole on the cytoplasmic side of the membrane. Recordings were made in response to steps to +40 mV (*left column*) and 0 mV (*right column*) from a holding voltage of −80 mV. The beginning of the trace corresponds to the start of depolarization. Zero current levels are marked by dashed lines. Recordings were filtered at 5 kHz and sampled at 25 kHz. (*B*) Representative first latency distributions in the presence of different concentrations of indole. Indole was applied to the cytoplasmic side of an inside-out patch containing only one channel. The distributions are shown for control, 0.5 mM and 1 mM indole for the data recorded at 40 mV (*left panel*) and 0 mV (*right panel*). Indole increases the time to the first opening of the channel so that the distributions appear to shift right. 100 to 200 traces at each voltage were used to build the distributions. (*C*) Normalized median values of the first latency distributions from several experiments. Data points represent the ratio of median first latency at a given concentration of indole to that in the control condition in each experiment. Different symbols represent different experiments. Data were recorded at 40 mV (*right panel*) and 0 mV (*left panel*) from several single-channel inside-out patches. Traces without openings were not included in the median determination.

closed durations before the first opening (first latency) are markedly increased by indole at both voltages shown.

Fig. 4 *B* compares the first latency distributions obtained at 40 and 0 mV from a representative experiment. Indole application increased the median first latency and the number of null sweeps where depolarization failed to elicit an opening. The relative increase in the first latency is further illustrated in Fig. 4 *C*. The median first latency measured in the presence of indole excluding the null sweeps was normalized by the control value in each experiment. The median first latency significantly increased with increasing concentrations of indole ($p = 0.011$ at 0 mV and $p = 0.018$ at 40 mV for 1 mM indole, paired *t*-test).

The effects of indole on the open and closed durations are summarized in Fig. 5. The open duration histograms before and after application of 1 mM indole were essentially identical (Fig. 5 *A*, *left*). In contrast, indole induced longer-lasting closed events (Fig. 5 *A*, *right*). The mean open and closed durations obtained from multiple experiments are summarized using different symbols in Fig. 5, *B* and *C*, respectively. Indole failed to alter the mean open duration ($p = 0.27$ at 0 mV and $p = 0.25$ at +40 mV for 1 mM indole, paired *t*-test) but significantly increased the mean closed duration ($p = 0.022$ at 0 mV and $p = 0.017$ at 40 mV for 1 mM indole, paired *t*-test).

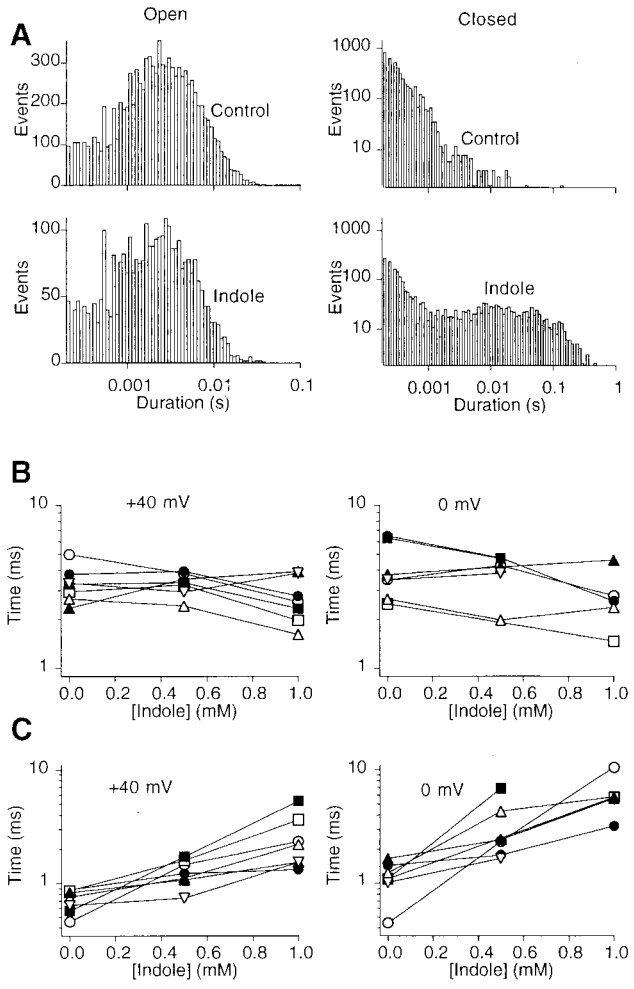

FIGURE 5 Indole increases the mean closed time of single ShBΔ 6–46:T449V channels. (*A*) Representative histograms of open (*left column*) and closed (*right column*) events in the control (*top row*) and in presence of 1 mM indole (*bottom row*). Data are derived from idealization of 40 to 50 of 1 s traces from a single channel inside-out patch. Indole was applied to the cytoplasmic side of the membrane. (*B*) Mean open durations in the presence of different concentrations of indole. Data shown are from several single-channel inside-out patches. Each experiment is shown by a distinct marker. Data values were obtained from idealized records by dividing the total time spend by the channel in the open state by the number of transitions to the closed state. Each point represents the average of 160 to 10,000 events (typically around 10^3 events). *Left panel* shows data at +40 mV, right panel at 0 mV. (*C*) Mean closed durations in the presence of different concentrations of indole. Data shown are from the same experiments as in *B* and were obtained and presented in the same way. The values on the plot were obtained by dividing the total time spent by the channel in the closed state by number of closed events.

Effects of indole on-gating currents

To better examine how indole alters the activation transitions among the closed states away from the open state, we recorded the gating currents from ShBΔ 6–46:T449V channels. Representative gating currents recorded before (*thick lines*) and after (*thin lines*) application of indole (4 mM) are shown in Fig. 6 *A*. Note that at 4 mM indole completely suppressed the ionic currents (Fig. 2). However, the on-gating currents before and after application of indole were essentially indistinguishable. The small decrease in the peak amplitude is probably attributable to rundown observed in the absence of potassium (Pardo et al., 1992). In contrast, indole markedly accelerated the overall time course of the off-gating currents. In the presence of 4 mM indole, a very fast transient appeared at the beginning of the off-gating current. The voltage dependence of the gating charge movement ($Q(V)$) was not noticeably altered by indole (Fig. 6 *B*).

Specificity to indole structure

To verify that the alterations in the Shaker channel gating induced by indole are caused by its specific structural features and not by a general effect of application of any small hydrophobic compound, we compared the effects of indole and quinoline (Fig. 7). Quinoline is similar to indole in its chemical structure, hydrophobicity, and size. However, despite the structural similarity, the effects of these compounds were readily distinguishable. The effects of quinoline and indole (1 mM) on the activation and deactivation time courses are compared in Fig. 7. Quinoline decreased the current amplitude in a time-independent manner. Furthermore, unlike indole, the quinoline block had no appreciable voltage dependence as indicated by the absence of time-dependent relaxation of the tail current.

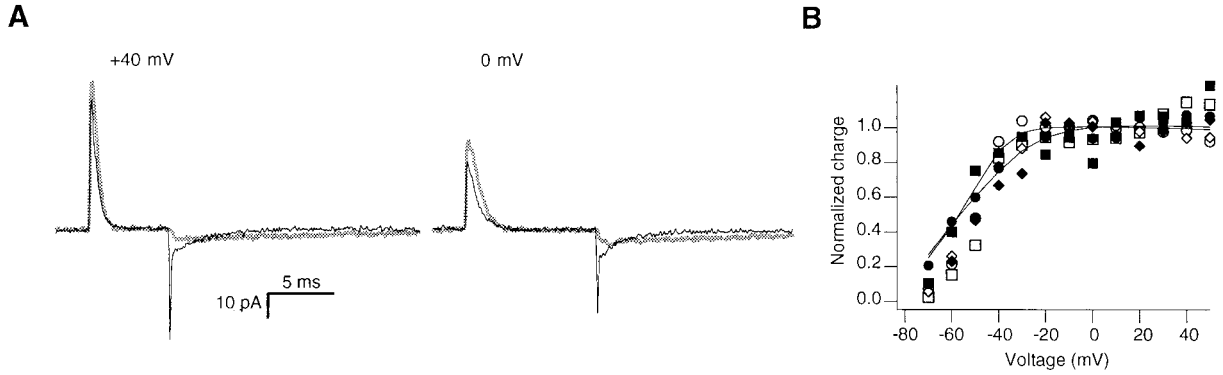

FIGURE 6 Indole does not noticeably alter on-gating currents. (*A*) Gating currents recorded from an inside-out patch in control (*thick lines*) and with 4 mM indole on the cytoplasmic side of the membrane (*thin lines*). On-gating currents at 40 mV (*left panel*) and at 0mV (*right panel*) are not affected by the presence of 4 mM indole (note that at this concentration indole completely suppresses ionic currents at these voltages; see Fig. 2). Gating currents were recorded by replacing Na^+ and K^+ ions in the external and internal solutions by NMG. Holding voltage was −80 mV. Leak currents were recorded in response to −50 mV pulse from the holding voltage of −120 mV. In some other experiments, leak subtraction was made using +50 mV pulse from the holding voltage of +50 mV. The result did not depend on the leak subtraction protocol used. Data were filtered at 5 kHz and sampled at 25 kHz. (*B*) Voltage dependence of normalized gating charge with and without 4 mM indole. The data values obtained by integrating on-gating currents. Data from three independent experiments are shown using different symbols. Empty symbols are control, filled symbols are the indole data. Smooth lines represent the model (Fig. 9) predictions with (*top*) and without (*bottom*) indole.

Indole does not alter currents through Kir2.1 (IRK1) inward-rectifier channels

We tested whether indole affected the inward rectifier Kir 2.1 (IRK1) channel (Kubo et al., 1993). The Kir2.1 lacks the S4 segment and it is not intrinsically voltage-activated (Fakler et al., 1995). The Kir2.1 channel was expressed in oocytes and the currents were recorded using TEV. Application of indole (1 mM) to the bath did not alter Kir2.1 currents in a noticeable way (Fig. 8). Similar results were obtained from 7 other cells tested. We verified that indole was effective in modifying ShBΔ 6–46:T449V currents when recorded with TEV (data not shown).

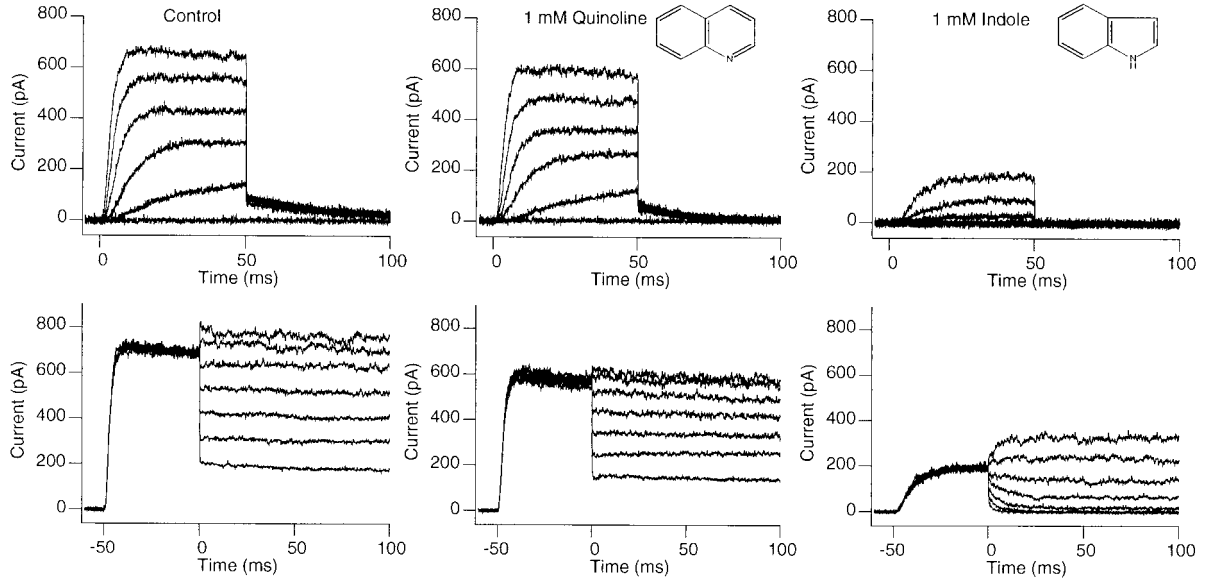

FIGURE 7 Comparison of the effects of indole and quinoline. Both compounds were applied to the intracellular side of the patch. The upper row shows currents elicited by depolarization to different voltages from −60 mV to +40 mV in 20 mV increments. The lower row shows currents at different voltages from −40 mV to +80 mV in 20 mV increments following prepulses to 50 mV for 50 ms to activate the channels. Time-dependent relaxation of the current which signifies voltage dependence of the drug action is absent in the data collected with quinoline.

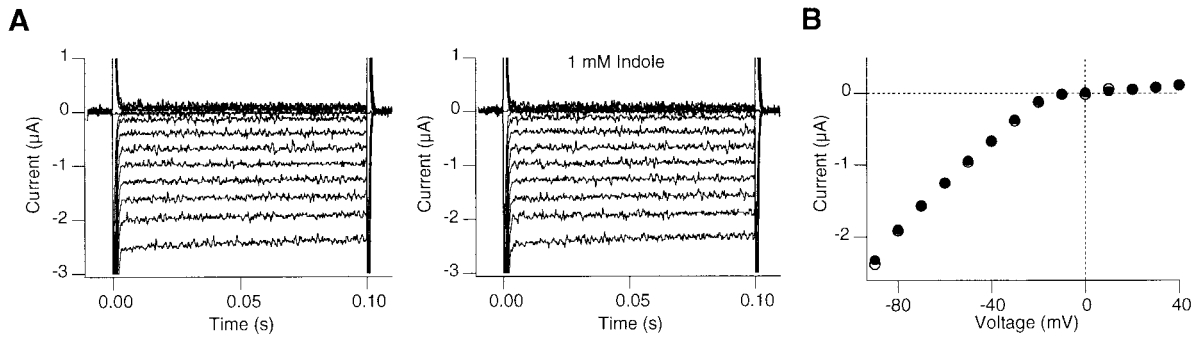

FIGURE 8 Indole does not alter currents through Kir2.1(IRK1) inward-rectifier channels. Currents were recorded using TEV. (*A*) Current traces recorded at −90 mV to +40 mV in 10 mV increments before (*left*) and after (*right*) addition of 1 mM indole. No leak/capacitative subtraction was made. Holding voltage was 0 mV. (*B*) Current-voltage curves before (*empty symbols*) and after (*filled symbols*) application of 1 mM indole. The external solution contained 140 mM KCl, 2 mM $MgCl_2$, 10 mM HEPES (pH 7.2; *N*-methyl glucamine).

DISCUSSION

We showed that indole alters gating kinetics of the Shaker potassium channel. At a given voltage, the macroscopic K^+ current is reduced by extracellular or intracellular application of indole. In the presence of indole, the macroscopic activation time course and the single-channel first latency distributions are also markedly slower. With increasing concentrations of indole, voltage dependence of the macroscopic conductance becomes less and less steep, such that the maximal conductance is achieved at more positive voltages. Despite the marked effect on the activation time course of the macroscopic ionic current, indole failed to modify the kinetics of on-gating currents and the voltage dependence of the gating charge movement even at the highest concentrations tested. Comparison of the two structurally similar compounds indole and quinoline shows that the gating alterations induced by indole are specific to its chemical structure and that they are unlikely to represent non-specific effects of application of small nonpolar compounds. Furthermore, indole failed to alter the Kir2.1 (IRK1) channel, suggesting that its effect is specific to voltage-gated K^+ channels.

The concentration dependence of the effect of indole to reduce the Shaker ionic currents at a given voltage is consistent with the idea that multiple, at least 3 molecules, of indole interact with the channel protein (Fig. 2 *D*). Considering the quadruple symmetry of the channel (MacKinnon, 1991), it is attractive to speculate that a single indole molecule interacts independently with each of the four subunits of the channel.

To elucidate the kinetic mechanism underlying the effects of indole on the Shaker channel, we used the model developed by Schoppa and Sigworth (Schoppa and Sigworth, 1998b) (SS model) shown in Fig. 9 *A*. This model satisfactorily describes many of the steady-state and kinetic properties of the Shaker channel without N-type inactivation (ShBΔ 6–46). The effect of indole was simulated by incorporating additional transitions and kinetic states reflecting the binding of indole to the channel.

We consider the possibility of indole directly affecting the open state of the channel unlikely because indole does not significantly alter the mean open time (Fig. 5 *A*). The slowing of activation by indole suggests that the closed states in the activation pathway before the open state may interact with indole. The SS model postulates that the activation process involves independent transitions among four distinct states, S0-S3, for each of the four subunits of the channel. These independent transitions are followed by a concerted transition into the last closed state C_{N-1}. The channel then enters the open state after making the second concerted transition from the C_{N-1} state.

The states S0-S3 have very short dwell times at positive voltages. Numerical simulations show that if indole binds exclusively to S0-S3 but not to C_{N-1}, the indole bound states are quickly vacated on depolarization and no appreciable steady-state block is observed. In contrast, C_{N-1} is directly connected to the open state and has a small but nonzero occupancy probability value even at positive voltages. Binding of indole to this state is sufficient to account for the steady-state decrease in the peak ionic current amplitude observed in our experiments as shown below.

Although the steady-state properties of the indole action could be accounted for by assuming that indole binds to C_{N-1}, the activation kinetics in the presence of indole suggests that it also interacts with some or all of the closed states S0, S1, S2, and S3. If indole binds only to C_{N-1}, a fraction of the channels would proceed directly to the open state. This fraction would manifest itself as an identifiable fast component in the macroscopic current activation and also in the first latency distribution. Our results do not show such fast components (Figs. 2 *A* and 4 *B*). In addition, if several indole molecules bind to C_{N-1} to account for the steep concentration dependence of the block, an apparent inactivation phase would be present in the macroscopic

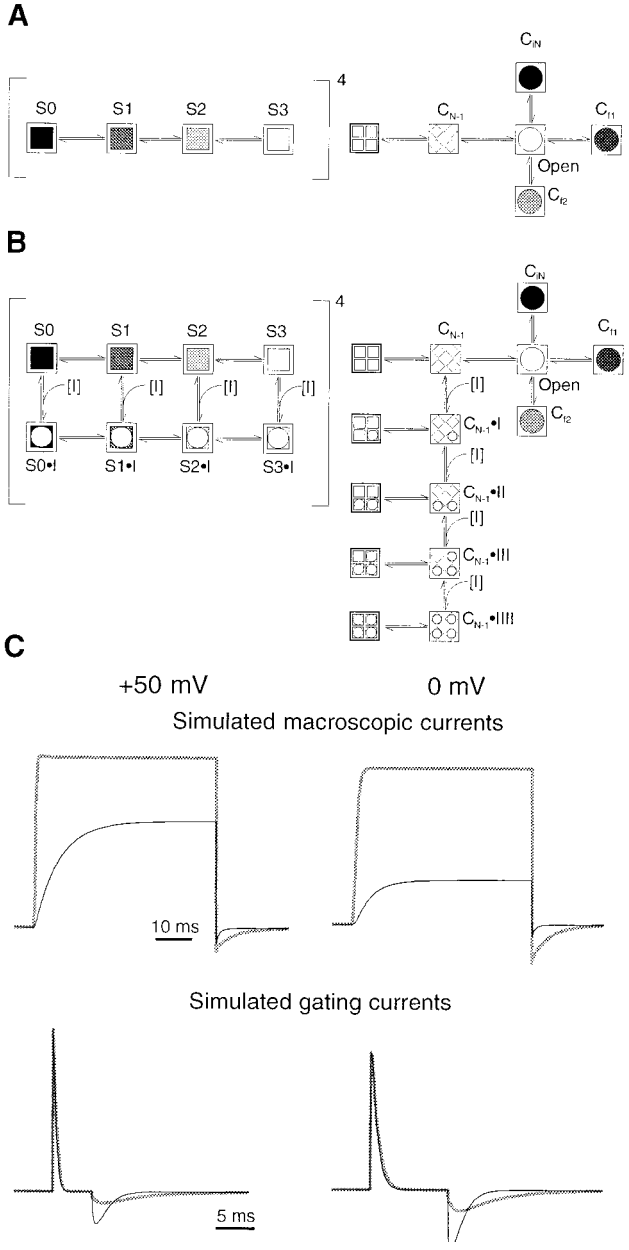

FIGURE 9 Kinetic model for the indole effect on the ShBΔ 6–46: T449V channel. (*A*) Kinetic model of Shaker channel gating from Schoppa and Sigworth (1998b). Symbols within the square brackets represent the states and transitions within a single subunit. Transitions on the right part represent concerted transitions of the channel as a whole. The starting state of the right part is the state when all four subunits are in state S3 as designated by four small symbols on the state icon. (*B*) Scheme representing the kinetic model of Shaker channel gating in the presence of indole. The model was built from the gating model presented in (*A*) by incorporating a transition from every state in the activation pathway to the indole bound state. (*C*) Macroscopic ionic currents (*top row*) and gating currents (*bottom row*) simulated using model in *B*. Traces are shown for depolarization to +50 mV (*left row*) and 0 mV (*right row*). Indole concentrations simulated correspond to 1 mM for macroscopic currents and 4 mM for gating currents. Traces in the presence of indole are shown using *thin lines* and those in control conditions using *thick lines*.

current. This inactivation would be produced by populating the non-conducting states with multiple indole molecules after the channel opens.

The voltage-dependent transitions from S0 to S3 are major determinants of the on-gating current kinetics. The observation that the on-gating currents are largely unaffected by indole indicates that these transitions proceed unhindered whether indole is bound to the channel or not. Binding to any subset of these closed states would noticeably alter the on-gating current kinetics. Thus, indole must bind to all of these closed states so that the voltage-dependent transitions among the indole-bound states are the same as those without indole.

The above considerations lead us to the kinetic model presented in Fig. 9 *B*. The model adds only a single indole binding transition to SS model. Since indole can bind to any of S0 through C_{N-1} states, this addition introduces the indole-bound states S0·I through C_{N-1}·I, designated by circle on top of original state symbol. The rate constants of the voltage dependent transitions (*horizontal arrows*) are the same in every column. Their values were taken from Schoppa and Sigworth (1998b). All vertical transitions are described by a single dissociation constant, obtained from the concentration dependence data.

This model accounts for all the major properties of the indole block: macroscopic and gating currents (Fig. 9 *C*), concentration dependence (Fig. 2 *B–D*), voltage dependence of conductance (Fig. 3 *B*), and voltage dependence of gating charge movement (Fig. 6 *B*). It also reproduces the effect of indole in the presence of N-type inactivation (Fig. 1 *B*, simulation not shown). At rest, the channel subunit may be found in the S0 or S0·I state. On depolarization, the channel proceeds through the top or bottom parallel activation pathway in Fig. 9 *B* (*left panel*) until it reaches the C_{N-1} family of states (Fig. 9 *B*, *right panel*), producing On-gating currents similar to those in the control condition (Fig. 9 *C*, *bottom*). From here on in the activation pathway, the rate of indole unbinding becomes rate-limiting, and slows the macroscopic activation time course and the first latency. In the presence of indole, the channel is trapped in the C_{N-1} family of closed states, which is normally very short-lived. The voltage dependence of steady-state block is determined by the voltage dependence of the equilibrium constant of the transition from C_{N-1} to O. The mean open time is not affected because the rate constants of the transitions away from the open state are unaltered. The overall deactivation time course is faster because the number of channels making the transition from C_{N-1} to O at negative voltages is decreased due to trapping in the C_{N-1} family of closed state by indole. The present model, based on that by Schoppa and Sigworth (1998b), does predict the observed acceleration of off-gating currents, but it fails to produce the rapid off-transient (Figs. 6 *A* and 8 *C*). This discrepancy may result from inability of the original model's to accurately predict

the gating transitions at very negative voltages as pointed out by its authors (Schoppa and Sigworth, 1998b).

One of the mechanistic interpretations consistent with this model is that indole could compete with the side chain of a tryptophan residue for its steric position in certain conformations. Indole could preoccupy the steric pocket intended for the tryptophan side chain and prevent the conformational rearrangement required for final concerted transition in the model. Tryptophan residues at positions 433 and 434 of the Shaker channel may be involved in such conformational rearrangements. These tryptophan residues are important in the stabilization of the selectivity filter as suggested by the crystal structure of the KcsA potassium channel (Doyle et al., 1998) and they are located near the structures that are known to undergo conformational changes during gating (Perozo et al., 1999). An implication of this hypothesis is that the stable selectivity filter structure is not present when the channel is closed at negative voltages but it is formed during the activation-gating process. And this formation involves repositioning of a tryptophan side chain.

Effects of indole similar to those observed with the Shaker channel may be found in other types of ion channels in which tryptophan side chains are repositioned during gating. Tryptophan side chain repositioning may also be involved in regulation in other proteins. For example, tryptophan at position 207 of transducin T α, which is conserved in all G proteins, changes its environment during activation of G protein, and is directly involved in G protein effector binding (Faurobert et al., 1993). It would be interesting to examine the effect of indole on the activation process of G proteins. Our results presented here show that indole effectively traps the activated channel in the transient C_{N-1} state. As in the Shaker potassium channel, indole might help to isolate a transient short-lived state in the enzyme reaction and may prove to be a useful tool in examining functional roles of tryptophan in protein function.

Supported in part by National Institutes of Health grant HL61645. VA was supported in part by fellowship from the American Heart Association, Heartland affiliate.

REFERENCES

Chung, S. H., and P. W. Gage. 1998. Signal processing techniques for channel current analysis based on hidden Markov models. *Methods Enzymol.* 293:420–437.

Creighton, T. E. 1983. Proteins. Structure and Molecular Principles. New York: W.H. Freeman and Company.

Doyle, D. A., J. Morais Cabral, R. A. Pfuetzner, A. Kuo, J. M. Gulbis, S. L. Cohen, B. T. Chait, and R. MacKinnon. 1998. The structure of the potassium channel: molecular basis of K+ conduction and selectivity. *Science.* 280:69–77.

Fakler, B., U. Brandle, E. Glowatzki, S. Weidemann, H. P. Zenner, and J. P. Ruppersberg. 1995. Strong voltage-dependent inward rectification of inward rectifier K+ channels is caused by intracellular spermine. *Cell.* 80:149–154.

Faurobert, E., A. Otto-Bruc, P. Chardin, and M. Chabre. 1993. Tryptophan W207 in transducin T alpha is the fluorescence sensor of the G protein activation switch and is involved in the effector binding. *EMBO J.* 12:4191–4198.

Glennon, R. A., and J. A. Rosecrans. 1982. Indolealkylamine and phenalkylamine hallucinogens: a brief overview. *Neurosci. Biobehav. Rev.* 6:489–497.

Guex, N., and M. C. Peitsch. 1997. SWISS-MODEL and the Swiss-PdbViewer: an environment for comparative protein modeling. *Electrophoresis.* 18:2714–2723.

Hamill, O. P., A. Marty, E. Neher, B. Sakmann, and F. J. Sigworth. 1981. Improved patch-clamp techniques for high-resolution current recording from cells and cell-free membrane patches. *Pflugers Arch.* 391:85–100.

Hess, P., J. B. Lansman, and R. W. Tsien. 1984. Different modes of Ca channel gating behaviour favoured by dihydropyridine Ca agonists and antagonists. *Nature.* 311:538–544.

Holmgren, M., P. L. Smith, and G. Yellen. 1997. Trapping of organic blockers by closing of voltage-dependent K+ channels: evidence for a trap door mechanism of activation-gating. *J. Gen. Physiol.* 109:527–535.

Hoshi, T., W. N. Zagotta, and R. W. Aldrich. 1990. Biophysical and molecular mechanisms of *Shaker* potassium channel inactivation. *Science.* 250:533–538.

Kubo, Y., T. J. Baldwin, Y. N. Jan, and L. Y. Jan. 1993. Primary structure and functional expression of a mouse inward rectifier potassium channel. *Nature.* 362:127–133.

Liu, Y., M. Holmgren, M. E. Jurman, and G. Yellen. 1997. Gated access to the pore of a voltage-dependent K+ channel. *Neuron.* 19:175–184.

Lopez-Barneo, J., T. Hoshi, S. H. Heinemann, and R. W. Aldrich. 1993. Effects of external cations and mutations in the pore region on C-type inactivation of Shaker potassium channels. *Receptors Channels.* 1:61–71.

MacKinnon, R. 1991. Determination of the subunit stoichiometry of a voltage-activated potassium channel. *Nature.* 350:232–235.

Methfessel, C., V. Witzemann, T. Takahashi, M. Mishina, S. Numa, and B. Sakmann. 1986. Patch clamp measurements on *Xenopus laevis* oocytes: currents through endogenous channels and implanted acetylcholine receptor and sodium channels. *Pflugers Arch.* 407:577–588.

Pang, D. C., and N. Sperelakis. 1983. Nifedipine, diltiazem, bepridil and verapamil uptakes into cardiac and smooth muscles. *Eur. J. Pharmacol.* 87:199–207.

Pardo, L. A., S. H. Heinemann, H. Terlau, U. Ludewig, C. Lorra, O. Pongs, and W. Stuhmer. 1992. Extracellular K^+ specifically modulates a rat brain K^+ channel. *Proc. Natl. Acad. Sci. U.S.A.* 89:2466–2470.

Perozo, E., D. M. Cortes, and L. G. Cuello. 1999. Structural rearrangements underlying K+-channel activation-gating. *Science.* 285:73–78.

Perozo, E., R. MacKinnon, F. Bezanilla, and E. Stefani. 1993. Gating currents from a nonconducting mutant reveal open-closed conformations in Shaker K^+ channels. *Neuron.* 11:353–358.

Schoppa, N. E., and F. J. Sigworth. 1998a. Activation of shaker potassium channels. I. Characterization of voltage-dependent transitions. *J. Gen. Physiol.* 111:271–294.

Schoppa, N. E., and F. J. Sigworth. 1998b. Activation of Shaker potassium channels. III. An activation-gating model for wild-type and V2 mutant channels. *J. Gen. Physiol.* 111:313–342.

Starkus, J. G., L. Kuschel, M. D. Rayner, and S. H. Heinemann. 1997. Ion conduction through C-type inactivated Shaker channels. *J. Gen. Physiol.* 110:539–550.

Windholz, M., editor. 1976. The Merck Index. Rahway, NJ: Merck and Co., Inc.

Yang, Y., Y. Yan, and F. J. Sigworth. 1997. How does the W434F mutation block current in Shaker potassium channels? *J. Gen. Physiol.* 109: 779–789.

Yellen, G. 1998. The moving parts of voltage-gated ion channels. *Q. Rev. Biophys.* 31:239–295.

Zagotta, W. N., T. Hoshi, J. Dittman, and R. W. Aldrich. 1994. Shaker potassium channel gating. II: Transitions in the activation pathway. *J. Gen. Physiol.* 103:279–319.

Zheng, J., and F. J. Sigworth. 1998. Intermediate conductances during deactivation of heteromultimeric Shaker potassium channels. *J. Gen. Physiol.* 112:457–474.